Journal of Power Sources 189 (2009) 888–893

Contents lists available at ScienceDirect

Journal of Power Sources

journal homepage: www.elsevier.com/locate/jpowsour

Influence of CaO on structure and electrical conductivity of pyrochlore-type $Sm_2Zr_2O_7$

Xiao-Liang Xia, Jia-Hu Ouyang*, Zhan-Guo Liu

Institute for Advanced Ceramics, Department of Materials Science, Harbin Institute of Technology, Harbin 150001, China

ARTICLE INFO

Article history:
Received 10 December 2008
Received in revised form
26 December 2008
Accepted 30 December 2008
Available online 14 January 2009

Keywords:
$(Sm_{1-x}Ca_x)_2Zr_2O_{7-x}$
Pyrochlore
Electrical conductivity
Impedance spectroscopy

ABSTRACT

$(Sm_{1-x}Ca_x)_2Zr_2O_{7-x}$ $(0 \le x \le 0.100)$ ceramics were prepared by a solid state reaction process at 1973 K for 10 h in air, and were characterized by X-ray diffraction (XRD) and scanning electron microscopy (SEM). $(Sm_{1-x}Ca_x)_2Zr_2O_{7-x}$ $(0 \le x \le 0.025)$ ceramics have a single phase of pyrochlore-type structure; however $(Sm_{1-x}Ca_x)_2Zr_2O_{7-x}$ $(0.050 \le x \le 0.100)$ consist of pyrochlore phase and a small amount of perovskite-like $CaZrO_3$. The electrical conductivity of $(Sm_{1-x}Ca_x)_2Zr_2O_{7-x}$ ceramics was investigated by complex impedance spectroscopy over a frequency range of 0.1 Hz to 20 MHz in the temperature range of 573–873 K. The measured electrical conductivity obeys the Arrhenius relation. Both the activation energy and pre-exponential factor for grain conductivity increase with increasing the CaO content; however, electrical conductivity of $(Sm_{1-x}Ca_x)_2Zr_2O_{7-x}$ decreases with increasing the CaO content, which is due to the increase in structural disordering at $0 \le x \le 0.025$ and the presence of the poorly conducting $CaZrO_3$ phase at $0.050 \le x \le 0.100$, respectively.

1. Introduction

In the past few years, pyrochlore compounds with the general formula $A_2B_2O_7$, where A is a trivalent rare-earth element and B is a tetravalent transition metal, are of great technological importance [1]. These compounds can be used as candidates for catalysts [2,3], nuclear waste disposal [4,5] and thermal barrier coatings (TBCs) [6], due to their interesting physical and chemical properties. Especially, their electrical properties depending on the composition and the degree of disorder on the cation sites [7] make them promising hosts for solid electrolytes in high-temperature fuel cells. Oxide-ion conductors of pyrochlore structure $A_2B_2O_7$ are potential candidates to substitute materials currently used in the fuel cells [8]. The advantages of lowering the operation temperature have attracted great interest worldwide. Enormous amounts of efforts have been made to improve ionic conductivity of the oxide electrolyte materials [9,10].

Among the pyrochlores, $Gd_2Zr_2O_7$ has been of keen concern due to its high oxide-ion conductivity at relatively low temperatures as compared with the commercially used electrolytes [11]. van Dijk et al. [12] found that the ionic conductivity of $Gd_2Zr_2O_7$ was the highest among all of the reported pyrochlores. There have been some efforts to improve the conductivity of $Gd_2Zr_2O_7$ by substitution at the Gd site. $Gd_2Zr_2O_7$ doped with 5 and 10 mol% Sr at the Gd site had a higher total-conductivity than pure $Gd_2Zr_2O_7$ in the temperature range of 773–1023 K [13]. Mandal et al. [14] prepared $(Gd_{1-x}Nd_x)_2Zr_2O_7$ $(0 \le x \le 1.0)$ by a solid state reaction route, and found a significant enhancement of ionic conductivity in $(Gd_{0.5}Nd_{0.5})_2Zr_2O_7$ at 622–696 K. Electrical properties were investigated in a La substituted fluorite-$Gd_2Zr_2O_7$, and a peak in ionic conductivity was found for the $(Gd_{0.8}La_{0.2})_2Zr_2O_7$ at 1073 K [15]. Díaz-Guillén et al. [16] substituted La for Gd in pyrochlore-type $(Gd_{1-x}La_x)_2Zr_2O_7$ solid solutions $(0 \le x \le 1.0)$ and found that ionic conductivity at temperatures of 773–1023 K was almost La-content independent for $x \le 0.4$. Liu et al. [17] synthesized $(Gd_{1-x}Sm_x)_2Zr_2O_7$ $(0 \le x \le 1.0)$ ceramics by the chemical-coprecipitation and calcination method, and obtained the highest electrical conductivity value at 873 K for $(Gd_{0.5}Sm_{0.5})_2Zr_2O_7$. Recently, the effect of homovalent A-site substitution on the electrical conductivity of pyrochlore-type $Gd_2Zr_2O_7$ was studied, and found that ionic conductivity remained almost constant or even increased slightly [18].

The electrical conductivity of $Sm_2Zr_2O_7$ pyrochlore phase was comparable to those of other good oxide-ion conductors in low-temperature regions [19]. However, to the best of our knowledge, there is no report to investigate the influence of divalent oxide doping on electrical conductivity of $Sm_2Zr_2O_7$ ceramic. In the present work, structure and electrical conductivity of pyrochlore-type $Sm_2Zr_2O_7$ doped with different contents of CaO were investigated.

2. Experimental procedure

In the present study $(Sm_{1-x}Ca_x)_2Zr_2O_{7-x}$ $(0 \le x \le 0.100)$ ceramics were synthesized by a solid state reaction process. The starting

* Corresponding author. Tel.: +86 451 86414291; fax: +86 451 86414291.
E-mail address: ouyangjh@hit.edu.cn (J.-H. Ouyang).

0378-7753/$ – see front matter © 2009 Elsevier B.V. All rights reserved.
doi:10.1016/j.jpowsour.2008.12.136

materials were samaria (Grirem Advanced Materials Co. Ltd., China; purity ≥99.9%), zirconia (Shenzhen Nanbo Structure Ceramics Co. Ltd., China; purity ≥99.9%) and calcia (Shanghai Fengxian Fengcheng Reagent Factory; analytical pure). All raw powders were first calcined at 1173 K for 2 h to remove adsorptive water in air before weighing. Samaria, zirconia and calcia powders in appropriate ratios were mechanically mixed for 24 h in absolute alcohol medium using zirconia milling media. The dried powder mixtures were molded by the uniaxial stress. Subsequently, the molded samples were further compacted by cold isostatic pressing at 280 MPa for 5 min. Finally, the compacts were pressureless-sintered at 1973 K for 10 h in air. The densities of the specimens were measured by using the Archimedes method.

The phases of sintered samples were characterized by a X-ray diffractometer (Rigaku, D/MAX 2200VPC, Japan) with Cu Kα radiation at a scan rate of 4° min^{-1} and slow step scans on the peak of $(622)_{Py}$ were conducted at a rate of 0.02°/3 s to calculate the lattice parameters of solid solutions using the least-squares method. The microstructure of ceramics was observed by scanning electron microscopy (SEM, CamScan MX 2600FE, UK). The specimens were polished, and then thermally etched at 1823 K for 1 h in air before SEM observations. Qualitative X-ray elemental analysis of various phases was carried out using SEM equipped with energy dispersive spectroscopy (EDS, Oxford Instruments INCA X-sight system, 7537, UK). Cylindrical pellet-form specimens with a diameter of 8 mm and a thickness of approximate 1 mm were machined from the sintered samples. Sample pellets were polished and cleaned with acetone in an ultrasonic cleaner. Both the flat surfaces of each pellet were coated with a conducting platinum paste. Each pellet was then heated to 1223 K for 2.5 h with a heating rate of 5 K min^{-1} in order to ensure good contact with the specimen surface. Impedance spectroscopy was carried out on a Solatron 1260 impedance analyzer with an applied voltage of 20 mV in the frequency range of 0.1 Hz to 20 MHz in air. Conductivity measurements were carried out during heating from 573 to 873 K at a 50 K interval with a heating rate of 5 K min^{-1} and a dwelling time of 15 min between consecutive measurements.

3. Results and discussion

The relative densities of sintered $(Sm_{1-x}Ca_x)_2Zr_2O_{7-x}$ samples used in this investigation are shown in Table 1. The relative densities of $(Sm_{1-x}Ca_x)_2Zr_2O_{7-x}$ ceramics are in the range of 96–98%. Fig. 1 shows the XRD patterns of $(Sm_{1-x}Ca_x)_2Zr_2O_{7-x}$ ceramics sintered at 1973 K for 10 h in air. It can be seen that all the samples except for $(Sm_{0.900}Ca_{0.100})_2Zr_2O_{6.900}$ have a single phase of pyrochlore structure, which is characterized by the presence of typical superstructure diffraction peaks at the 2θ values of about 14° (1 1 1), 28° (3 1 1), 37° (3 3 1), 45° (5 1 1) and 51° (5 3 1) using Cu Kα radiation [20,21]. $(Sm_{0.900}Ca_{0.100})_2Zr_2O_{6.900}$ consists of pyrochlore structure and minor perovskite-like $CaZrO_3$ as a second phase as shown in Fig. 1. As compared with undoped $Sm_2Zr_2O_7$ $(Sm_{1-x}Ca_x)_2Zr_2O_{7-x}$ $(0.025 \le x \le 0.075)$ ceramics exhibit a single phase of pyrochlore structure. The peaks slightly shift towards a low angle region, which indicates the solution of CaO into the pyrochlore phase. The ionic

Table 1
Relative densities of $(Sm_{1-x}Ca_x)_2Zr_2O_{7-x}$ ceramics used in this investigation.

Ceramic materials	Composition (mol%)			Relative densities (%)
	ZrO_2	$SmO_{1.5}$	CaO	
$Sm_2Zr_2O_7$	50.00	50.00	0	96.3
$(Sm_{0.975}Ca_{0.025})_2Zr_2O_{6.975}$	50.00	48.75	1.25	97.1
$(Sm_{0.950}Ca_{0.050})_2Zr_2O_{6.950}$	50.00	47.50	2.50	97.5
$(Sm_{0.925}Ca_{0.075})_2Zr_2O_{6.925}$	50.00	46.25	3.75	97.8
$(Sm_{0.900}Ca_{0.100})_2Zr_2O_{6.900}$	50.00	45.00	5.00	96.5

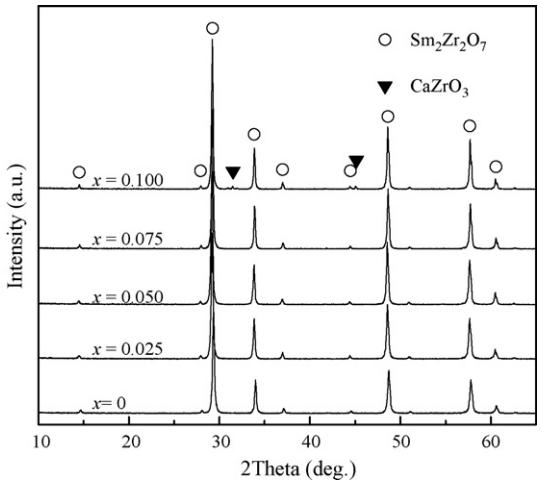

Fig. 1. XRD patterns of $(Sm_{1-x}Ca_x)_2Zr_2O_{7-x}$ ceramics sintered at 1973 K for 10 h.

radius of Ca^{2+} and Sm^{3+} are 1.120 and 1.079 Å in an eightfold coordination, respectively [22]. The heterovalent-doped $Sm_2Zr_2O_7$ with CaO increases the lattice parameters of $Sm_2Zr_2O_7$ when Ca occupies the Sm site, so a peak shift is observed. Slow step scans on the peak of $(622)_{Py}$ at a rate of 0.02°/3 s are carried out to calculate the lattice parameters of solid solutions. Fig. 2 shows XRD patterns of ceramics in a 2θ range of 56–60°. As contrasted with the $Sm_2Zr_2O_7$ ($x = 0$), the $(622)_{Py}$ peak of different CaO-doped $(Sm_{1-x}Ca_x)_2Zr_2O_{7-x}$ ceramics from $x = 0.025$ to $x = 0.100$ shifts slightly to the low angle region as shown in Fig. 2(a). The lattice parameters of different CaO-doped $(Sm_{1-x}Ca_x)_2Zr_2O_{7-x}$ ceramics calculated from

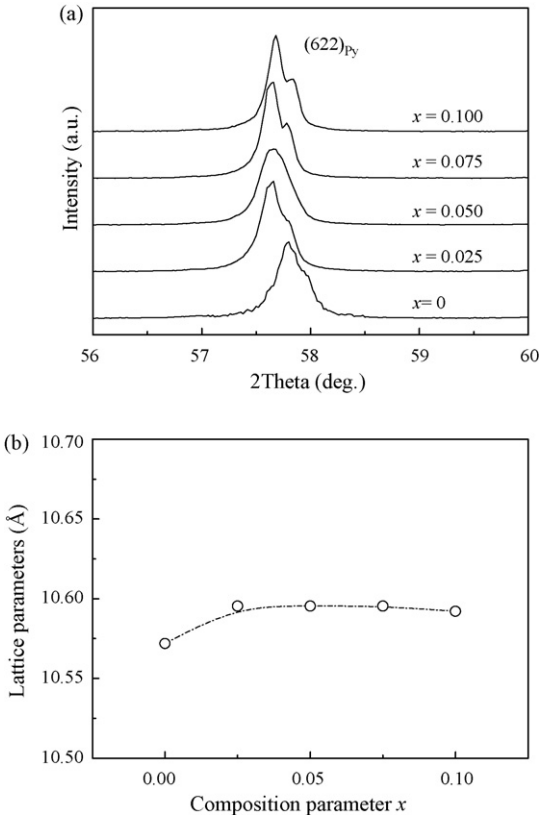

Fig. 2. Slow step-scan XRD patterns and calculated lattice parameters of $(Sm_{1-x}Ca_x)_2Zr_2O_{7-x}$ ceramics: (a) the $(622)_{Py}$ peak in a 2θ range of 56–60°; (b) lattice parameters derived from (a) above.

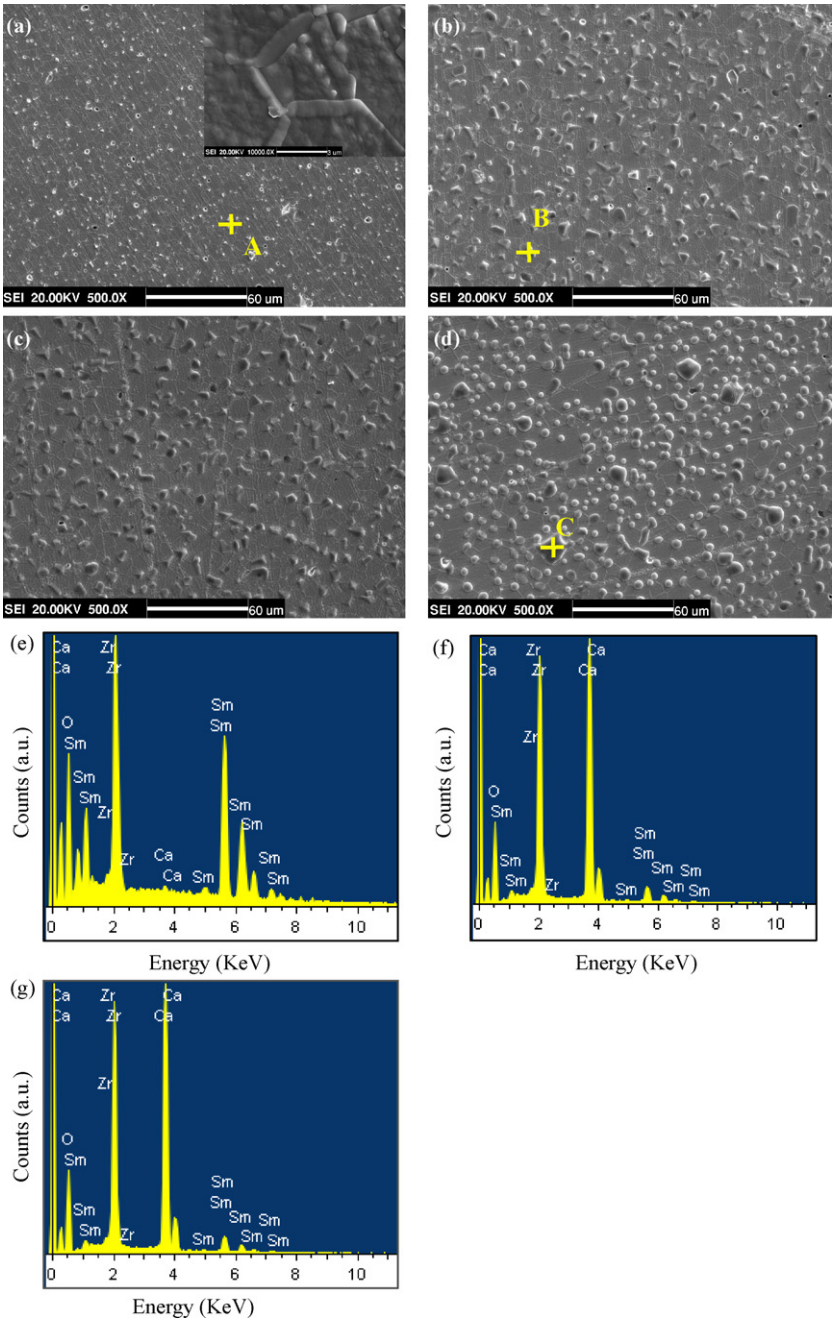

Fig. 3. SEM micrographs showing the microstructure of sintered $(Sm_{1-x}Ca_x)_2Zr_2O_{7-x}$ samples: (a) $x = 0.025$; (b) $x = 0.050$; (c) $x = 0.075$; (d) $x = 0.100$; (e–g) EDS at different positions of A–C, respectively; the inset in (a) shows a high-magnification image.

their $(622)_{Py}$ diffraction peaks of pyrochlore-type unit cell are depicted in Fig. 2(b). It can be seen that the lattice parameters of $(Sm_{1-x}Ca_x)_2Zr_2O_{7-x}$ initially increase and then remain almost constant with further increase of the CaO content. This indicates that the solubility of CaO in pyrochlore-type $Sm_2Zr_2O_7$ is very low.

Fig. 3 presents SEM micrographs for $(Sm_{1-x}Ca_x)_2Zr_2O_{7-x}$ $(0.025 \le x \le 0.100)$ ceramics. The SEM images of sintered $(Sm_{1-x}Ca_x)_2Zr_2O_{7-x}$ samples indicate that all of them have a high relative density. From Fig. 3(a), the grain is basically uniform for $(Sm_{0.975}Ca_{0.025})_2Zr_2O_{6.975}$ $(x = 0.025)$ with some pores. No second phase is identified in the SEM micrograph, which is confirmed by the corresponding EDS analysis as shown in Fig. 3(e). The inset in Fig. 3(a) showing a high-magnification image also confirms this point. However, for $x = 0.050$, from Fig. 3(b) the second phase can be clearly observed at the grain boundaries of matrix as contrasted with the results obtained at $x = 0.025$, although the XRD patterns for $(Sm_{1-x}Ca_x)_2Zr_2O_{7-x}$ $(0.050 \le x \le 0.075)$ do not clearly identify the existence of the second phase. This indicates that the amount of the second phase is low and is not able to be identified by XRD. From the SEM micrographs taken from Fig. 3(b)–(d), it is evident that the amount of the second phase increases with increasing the CaO content. The corresponding EDS analysis in Fig. 3(g) indicates that the composition of the second phase contains more Ca but less Sm, which is similar to that in Fig. 3(f). In combination with Fig. 2, it can be inferred that the second phase is perovskite-like $CaZrO_3$ and the solubility limit of CaO in pyrochlore-type $Sm_2Zr_2O_7$ at 1973 K is $x = 0.025$.

The impedance spectroscopy at different temperatures was plotted in the complex plane for all of the samples. Fig. 4 shows

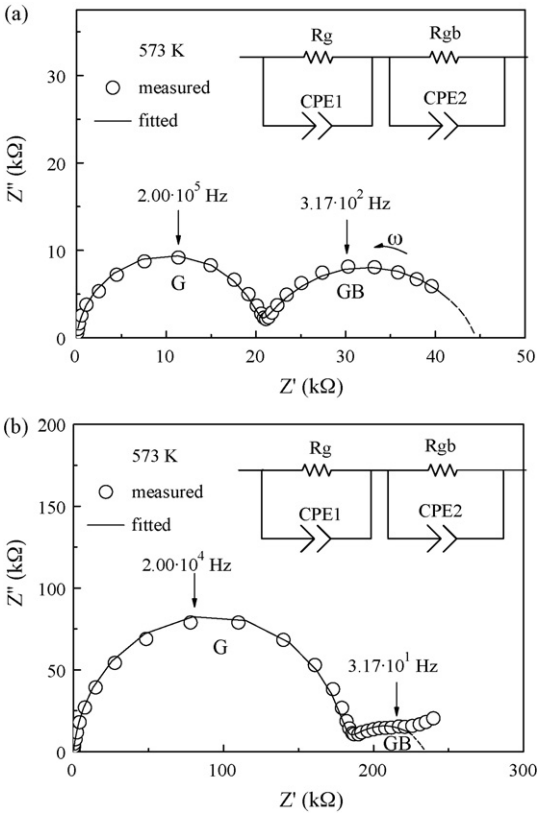

Fig. 4. Complex impedance plots and corresponding equivalent circuit in the complex plain at 573 K for different $(Sm_{1-x}Ca_x)_2Zr_2O_{7-x}$ samples: (a) $Sm_2Zr_2O_7$ and (b) $(Sm_{0.925}Ca_{0.075})_2Zr_2O_{6.925}$. The grain (G) and grain-boundary (GB) contributions are indicated.

typical complex impedance plots measured at 573 K in air for $Sm_2Zr_2O_7$ and $(Sm_{0.925}Ca_{0.075})_2Zr_2O_{6.925}$ where two main features are evident. Equivalent circuit used and corresponding fitted results are also shown in Fig. 4. As it can be seen that the results of the fit are very close to measured results. Two distinct contributions in the form of semicircular arcs are identified in Fig. 4. The complete high frequency semicircle corresponds to the grain impedance, the incomplete low frequency semicircle represents the grain-boundary impedance. These two contributions are separated by fitting semicircles to each of the arcs. From Fig. 4(a), capacitance values obtained for the high frequency and low frequency arcs are 6.45×10^{-11} and 2.07×10^{-7} F cm^{-1} at 573 K, which corresponds to the grain and grain-boundary contributions for $Sm_2Zr_2O_7$, respectively. However, for $(Sm_{0.925}Ca_{0.075})_2Zr_2O_{6.925}$ ceramics, capacitance values obtained for the high frequency and low frequency arcs are 5.80×10^{-11} and 3.39×10^{-7} F cm^{-1}, respectively, as shown in Fig. 4(b). At a given measurement temperature, an equivalent circuit model consists of parallel resistance–capacitance was applied to fit the experimental data and reproduce impedance plots [23]. The grain resistance values, R_g are determined from the intercepts of high frequency range semicircles on the Z' axes [24]. In general, grain resistance values R_g can be converted to electrical conductivity σ_g using the following equation:

$$\sigma_g = \frac{l}{R_g S} \tag{1}$$

where l is the sample thickness and S is the electrode area of the sample surface. In this way, the electrical conductivity at different temperatures can be obtained. The temperature dependence of the grain conductivity and grain-boundary conductivity of samples with Ca concentrations is analyzed by using an Arrhenius-type equation:

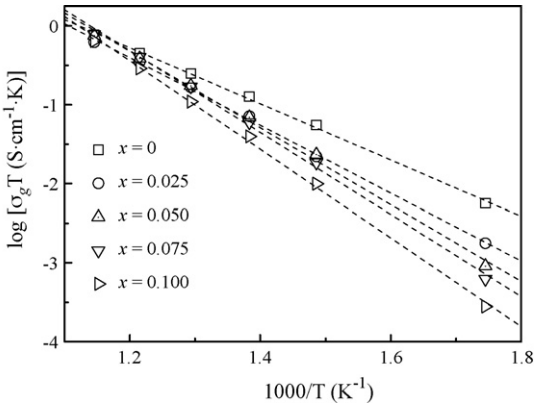

Fig. 5. Arrhenius plots of grain (G) conductivity for $(Sm_{1-x}Ca_x)_2Zr_2O_{7-x}$ ceramics.

$$\sigma_g T = \sigma_0 \ \exp\left(\frac{-E}{k_B T}\right) \tag{2}$$

where σ_0 is pre-exponential factor, which is a measurement of the effective number of mobile oxide ions, E denotes the activation energy for the electrical conduction process, k_B is the Boltzmann constant, and T is absolute temperature. Fig. 5 presents the Arrhenius plots of the grain conductivity of $(Sm_{1-x}Ca_x)_2Zr_2O_{7-x}$ ceramics. The values of activation energy E_g and pre-exponential factor σ_{0g} for each composition are calculated from the slope and the intercept of the linear fits in the Arrhenius plots as shown in Fig. 5, respectively. The activation energy E_g and pre-exponential factor σ_{0g} of $(Sm_{1-x}Ca_x)_2Zr_2O_{7-x}$ ceramics for the grain conductivity as a function of CaO content are shown in Fig. 6. The activation energy E_g steadily increases with increasing the CaO content. Similar observations were made in the case of $(Gd_{1-x}Ca_x)_2Zr_2O_{7-x}$ $(0 \le x \le 0.100)$ [25]. The activation energy E_g increases with increasing the CaO content. This indicates that the energy barrier, which oxide ions must overcome to hop to neighboring vacant sites, becomes high with the increase of the CaO content. The activation energy E_g of pyrochlore-type $Sm_2Zr_2O_7$ in this study is 0.71 eV, which is slightly lower than Liu's results (0.73 eV) [17]. The pre-exponential factor σ_{0g} has a similar trend to activation energy E_g. It gradually increases with increasing the CaO content, indicating that the effective number of mobile oxide ions increases due to the Ca substitution for Sm in $(Sm_{1-x}Ca_x)_2Zr_2O_{7-x}$ ceramics.

Fig. 5 also compares the grain conductivity of $Sm_2Zr_2O_7$ with that of the CaO-doped samples. Grain conductivity decreases with increasing the CaO content. From the X-ray diffraction patterns,

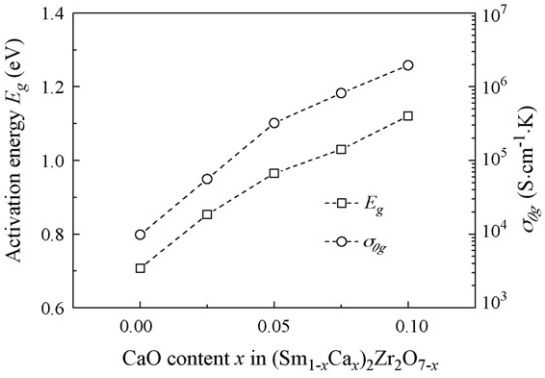

Fig. 6. Activation energy E_g and pre-exponential factor σ_{0g} of $(Sm_{1-x}Ca_x)_2Zr_2O_{7-x}$ ceramics for the grain conductivity as a function of CaO content.

the solubility limit of CaO in $Sm_2Zr_2O_7$ at 1973 K is $x = 0.025$. An increased disordering of structure can be brought about by cation disordering (metal ions occupying the cation sites in a statistical manner) due to compositional changes [13]. With increasing the incorporation of CaO in pyrochlore phase, the number of vacancies at the oxide-ion sites increases in order to maintain charge balance. The increased number of oxide-ion vacancies is reflected in CaO-doped $Sm_2Zr_2O_7$; there is an increase in the pre-exponential factor. The increase in σ_{0g} would lead to an increase in conductivity. However, it also increases the activation energy E_g, since the low energy pathways due to the ordered cation sublattice are removed by the disordering. The increase in E_g would hinder the oxide-ion migration, so these two processes are competing. The drop in grain conductivity is attributed to the fact that the increase in E_g compensates for increase in the number of mobile species, thus decreasing the ease with which the ions can migrate. This indicates that the structure becomes progressively disordered [25]. Increasing the number of oxygen vacancies to increase σ_{0g} leads to undesired increase in E_g and eventually to low values of conductivity [26]. With further increasing the CaO content ($0.050 \le x \le 0.100$), both the pre-exponential factor and the activation energy increase, and the conductivity decreases with increasing the CaO content. This is due to the presence of the poorly conducting $CaZrO_3$ phase at the grain boundaries of $(Sm_{1-x}Ca_x)_2Zr_2O_{7-x}$ solid solutions. Dudek and Drożdż-Cieśla [27] found the pure $CaZrO_3$ exhibited low electrical conductivity (1.1×10^{-6} S cm^{-1}) and high activation energy at 1273 K. In the case of oxide-ion conducting electrolytes, a composite system such as the dispersion of perovskite phase $CaZrO_3$ into fluorite-type calcia stabilized zirconia did not exhibit enhanced conductivity [28]. The decrease in grain conductivity occurs in this study, depending upon dispersing small quantities of $CaZrO_3$ as an inert phase in a solid electrolyte.

Fig. 7 shows the variations of grain conductivity of $(Sm_{1-x}Ca_x)_2Zr_2O_{7-x}$ ceramics as a function of the CaO content. Apparently, the grain conductivity increases with increasing temperature for each composition, which indicates that ionic diffusion in this series is thermally activated. With the increase of the CaO content, the grain conductivity σ_g decreases from pure $Sm_2Zr_2O_7$ ($x = 0$) to $(Sm_{0.900}Ca_{0.100})_2Zr_2O_{6.900}$ ($x = 0.100$). The electrical conductivity of the pyrochlore-type $Sm_2Zr_2O_7$ system is not improved by doping different contents of CaO at the Sm sites.

Fig. 8 represents the effect of increasing the CaO content on the grain-boundary conductivity of $(Sm_{1-x}Ca_x)_2Zr_2O_{7-x}$ series at different temperatures. It can be seen that the grain-boundary conductivity of $(Sm_{1-x}Ca_x)_2Zr_2O_{7-x}$ ($0.025 \le x \le 0.100$) series decrease when CaO is doped into the pyrochlore structure of pure $Sm_2Zr_2O_7$. Clearly, a distinct decrease in grain-boundary conductivity of

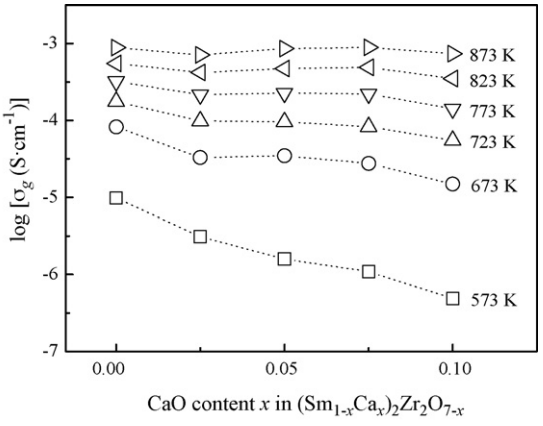

Fig. 7. Variations of the grain (G) conductivity of $(Sm_{1-x}Ca_x)_2Zr_2O_{7-x}$ ceramics as a function of CaO content.

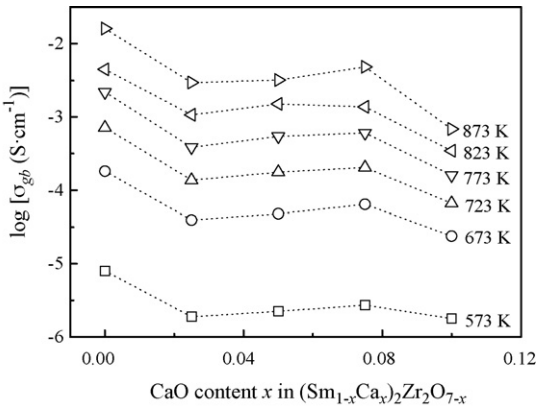

Fig. 8. Variations of the grain-boundary (GB) conductivity of $(Sm_{1-x}Ca_x)_2Zr_2O_{7-x}$ ceramics as a function of CaO content.

$(Sm_{1-x}Ca_x)_2Zr_2O_{7-x}$ is found at the x values of 0.025 and 0.100 at different temperature levels, which corresponds to the solubility limit of CaO in $Sm_2Zr_2O_7$ and the rapid growth of poorly conducting $CaZrO_3$ phase at the grain boundaries, respectively. The grain-boundary conductivity of CaO-doped $Sm_2Zr_2O_7$ is lower than that of pure $Sm_2Zr_2O_7$, which is due to the presence of both the CaO-doped pyrochlore structure and the poorly conducting $CaZrO_3$ phase. Here, the perovskite distributed at the grain boundaries of pyrochlore phase does not enhance conductivity.

4. Conclusions

(1) $(Sm_{1-x}Ca_x)_2Zr_2O_{7-x}$ ($0 \le x \le 0.025$) exhibit a single phase of pyrochlore-type structure. However, $Sm_{2-x}Ca_xZr_2O_{7-x}$ ($0.050 \le x \le 0.100$) ceramics consist of pyrochlore phase and a small amount of perovskite-like $CaZrO_3$. The amount of the second phase increases with increasing the dopant concentration. The solubility limit of CaO in pyrochlore-type $Sm_2Zr_2O_7$ at 1973 K is $x = 0.025$.

(2) The grain conductivity of $(Sm_{1-x}Ca_x)_2Zr_2O_{7-x}$ ($0 \le x \le 0.100$) ceramics decreases with the Ca substitution for Sm in the temperature range of 573–873 K. The activation energy E_g and pre-exponential factor σ_{0g} increase steadily as the CaO content increases.

(3) As contrasted with undoped $Sm_2Zr_2O_7$ ceramics, the decrease in grain- and grain-boundary conductivity of $(Sm_{0.975}Ca_{0.025})_2Zr_2O_{6.975}$ ($x = 0.025$) is discussed in terms of the increase in structural disordering. However, for $(Sm_{1-x}Ca_x)_2Zr_2O_{7-x}$ ($0.050 \le x \le 0.100$), the decrease in grain conductivity is due to the presence of the poorly conducting $CaZrO_3$ phase at the grain boundaries of CaO-doped pyrochlore-type structure.

Acknowledgements

The authors would like to thank the financial support from the Program of Excellent Teams in Harbin Institute of Technology (HIT) and the Start-up Program for High-level HIT Faculty Returned from Abroad.

References

[1] R.C. Ewing, W.J. Weber, J. Lian, J. Appl. Phys. 95 (2004) 9549.
[2] J.M. Sohn, S.I. Woo, Catal. Lett. 79 (2002) 45–48.
[3] J.M. Sohn, M.R. Kim, S.I. Woo, Catal. Today 83 (2003) 289–297.
[4] J. Lian, S.V. Yudintsev, S.V. Stefanovsky, L.M. Wang, R.C. Ewing, J. Alloys Compd. 444–445 (2007) 429–433.
[5] S. Lutique, D. Staicu, R.J.M. Konings, V.V. Rondinella, J. Somers, T. Wiss, J. Nucl. Mater. 319 (2003) 59–64.

[6] R. Vassen, X.Q. Cao, F. Tietz, D. Basu, D. Stőver, J. Am. Ceram. Soc. 83 (2000) 2023–2028.
[7] J. Chen, J. Lian, L.M. Wang, R.C. Ewing, L.A. Boatner, Appl. Phys. Lett. 79 (2001) 1989.
[8] M.A. Subramanian, G. Aravamudan, G.V. Subba Rao, Prog. Solid State Chem. 15 (1983) 55–143.
[9] J.W. Fergus, J. Power Sources 162 (2006) 30–40.
[10] S. Hui, J. Roller, S. Yick, X. Zhang, C. Decès-Petit, Y. Xie, R. Maric, D. Ghosh, J. Power Sources 172 (2007) 493–502.
[11] M.R. Díaz-Guillén, K.J. Moreno, J.A. Díaz-Guillén, A.F. Fuentes, K.L. Ngai, J. Garcia-Barriocanal, J. Santamaria, C. Leon, Phys. Rev. B 78 (2008) 104304.
[12] T. van Dijk, K.J. de Vries, A.J. Burggraaf, Phys. Status Solidi A 58 (1980) 115–125.
[13] K.V.G. Kutty, C.K. Mathews, T.N. Rao, U.V. Varadaraju, Solid State Ionics 80 (1995) 99–110.
[14] B.P. Mandal, S.K. Deshpande, A.K. Tyagi, J. Mater. Res. 23 (2008) 911–916.
[15] J.A. Díaz-Guillén, M.R. Díaz-Guillén, J.M. Almanza, A.F. Fuentes, J. Santamaría, C. León, J. Phys. Condens. Matter. 19 (2007) 356212.
[16] J.A. Díaz-Guillén, M.R. Díaz-Guillén, K.P. Padmasree, A.F. Fuentes, J. Santamaría, C. León, Solid State Ionics 179 (2008) 2160–2164.
[17] Z.-G. Liu, J.-H. Ouyang, Y. Zhou, X.-L. Xia, J. Power Sources 185 (2008) 876–880.
[18] J.A. Díaz-Guillén, A.F. Fuentes, M.R. Díaz-Guillén, J.M. Almanza, J. Santamaría, C. León, J. Power Sources 186 (2009) 349–352.
[19] K. Shinozaki, M. Miyauchi, K. Kuroda, O. Sakurai, N. Mizutani, M. Kato, J. Am. Ceram. Soc. 62 (1979) 538–539.
[20] Z.-G. Liu, J.-H. Ouyang, Y. Zhou, J. Alloys Compd 472 (2009) 319–324.
[21] Z.-G. Liu, J.-H. Ouyang, Y. Zhou, J. Li, X.-L. Xia, J. Eur. Ceram. Soc. 29 (2009) 647–652.
[22] G.S. Rohrer, Structure and Bonding in Crystalline Materials, Cambridge University Press, Cambridge, 2004, pp. 521–525.
[23] J.R. Macdonald, W.B. Johnson, Fundamentals of impedance spectroscopy, in: E. vBarsoukov, J.R. Macdonald (Eds.), Impedance Spectroscopy: Theory, Experiment and Applications, second edition, John Wiley & Sons, Inc., New Jersey, 2005, pp. 1–26.
[24] M.H. Abdullah, A.N. Yussof, J. Mater. Sci. 32 (1997) 5817–5823.
[25] T. Fournier, J.Y. Nots, J. Muher, J.C. Joubert, Solid State Ionics 15 (1985) 71–74.
[26] A.V. Chadwick, Nature 408 (2000) 925–926.
[27] M. Dudek, E. Drożdż-Cieśla, J. Alloys Compd. (2008), doi:10.1016/j.jallcom.2008.08.020.
[28] C.B. Alcock, J. Alloys Compd. 197 (1993) 217–227.